A Double Role for a Strictly Conserved Serine: Further Insights into the dUTPase Catalytic Mechanism

Lorena González Palmén,[‡] Kristian Becker,[§] Leif Bülow,[§] and Jan-Olov Kvassman*[,‡]

Department of Chemistry and Biomedical Sciences, School of Pure and Applied Natural Sciences, University of Kalmar, Kalmar, Sweden, and Department of Pure and Applied Biochemistry, Lund University, Lund, Sweden

Received February 26, 2008; Revised Manuscript Received May 19, 2008

ABSTRACT: Ser72 at the active site of the *Escherichia coli* dUTPase has been mutated to an alanine, and the properties of the mutant have been investigated. The serine is absolutely conserved among the monomeric and trimeric dUTPases (including the bifunctional dCTP deaminase:dUTPases), and it has been proposed to promote catalysis by balancing negative charge at the oxygen that bridges the α- and *β*-phosphorus of the substrate. In all reported complexes of dUTPases with the substrate analogue α,*β*-imido-dUTP·Mg, the serine *β*-OH is indeed hydrogen bonded to the α,*β*-bridging nitrogen of the analogue. However, in the complex of the Asp90 → Asn mutant dUTPase with the true substrate dUTP·Mg, the serine *β*-OH points in the opposite direction and may form a hydrogen bond to Asn84 at the bottom of the pyrimidine pocket. Here we show that the replacement of the *β*-OH by hydrogen reduces k_{cat} from 5.8 to 0.008 s^{-1} but also k_{-1}, the rate of substrate dissociation, from 6.2 to 0.1 s^{-1} ($K_M = 6 \times 10^{-9}$ M). We conclude that the serine *β*-OH exercises both ground state (GS) destabilization and transition state (TS) stabilization, effects not usually linked to a single residue. With experimental support, we argue that the *β*-OH destabilizes the GS by imposing conformational constraints on the enzyme and that formation of the TS depends on a rotation of the serine side chain that not only relieves the constraints but brings the *β*-OH into a position where it can electrostatically stabilize the TS. This rotation would also allow the *β*-OH to promote both deamination and hydrolysis in the bifunctional deaminases. We find that the *E. coli* dUTPase does not catalyze the hydrolysis of the α,*β*-imido-dUTP·Mg, suggesting that the analogue provides the hydrogen in the bond to the serine *β*-OH.

The ubiquitous enzyme dUTP[1] diphosphatase (EC 3.6.1.23), or dUTPase, catalyzes the hydrolysis of the $dUTP^{4-}$ Mg^{2+} complex (dUTP·Mg) into dUMP and pyrophosphate. This reaction effectively reduces the cellular dUTP/dTTP ratio by removing dUTP and providing dUMP as the precursor for dTTP synthesis via the thymidylate synthase pathway. An elevated dUTP/dTTP ratio results in fragmentation of nascent DNA and cell death. For this reason, members of the dUTPase family of enzymes are currently recognized as potential targets for drugs in the treatment of cancers and infectious diseases (*1–3*).

The human dUTPase (*4*) and most bacterial (*5, 6*) and viral dUTPases (*7–9*) are C_3-symmetric entities with the three substrate pockets located at the subunit interfaces (Figure 1A). An unusual feature is that all subunits contribute to each site. The C-terminus of one subunit is integrated as a *β*-strand with its neighbor and extends from this to interact with the remote site. The representation of the *Escherichia coli* dUTPase trimer shown in Figure 1A does not include the last 15 residues of the C-termini. This part of the subunit was not resolved in the crystal study (*10*). It constitutes a flexible arm which becomes ordered upon formation of the productive enzyme substrate complex (*6*). Despite the intertwined nature of the trimer, the sites appear independent in substrate binding and catalysis (*11*).

Dimeric dUTPases have been found in protozoans (*12, 13*) and bacteria (*14*). They show no homology to the trimeric dUTPases and catalyze the reaction by a different mechanism. In contrast, the monomeric dUTPases, which only occur in the herpes viruses, such as the Epstein−Barr virus (EBV), have a single active site that mimics in detail that of the trimeric dUTPases (*15*). The monomeric and trimeric dUTPases catalyze a direct in-line nucleophilic attack by water on the α-phosphorus with displacement of pyrophosphate. The substrate water becomes enclosed at the active site upon formation of the productive complex and does not share its protons with the reaction medium. Instead, a strictly conserved aspartate, D90 in the *E. coli* dUTPase, activates the water by temporarily harboring one of its protons (*6, 10, 11*). Apart from the aspartate, a strictly conserved serine, S72 in the *E. coli* dUTPase, at the opposite side of the reactive center has been proposed to play a direct role in dUTPase catalysis (Figure 1B,C) (*6*).

* Address correspondence to this author. Tel: +46 480446290. Fax: +46 480446262. E-mail: jan.kvassman@hik.se.

‡ University of Kalmar.

§ Lund University.

[1] Abbreviations: dUTP, deoxyuridine triphosphate; dUMP, deoxyuridine monophosphate; dUDP, deoxyuridine diphosphate; dTTP, deoxythymidine triphosphate; dCTP, deoxycytidine triphosphate; α,*β*-imido-dUTP, 2′-deoxyuridine 5′-(α,*β*-imido)triphosphate; ATP, adenosine triphosphate; IPTG, isopropyl *β*-D-thiogalactoside; EDTA, ethylenediaminetetraacetic acid; EGTA, ethylene glycol tetraacetic acid; DTT, 1,4-dithiotheitol; PMSF, phenylmethanesulfonyl fluoride; GuHCl, guanidine hydrochloride.

10.1021/bi800325j CCC: $40.75
Published on Web 07/03/2008

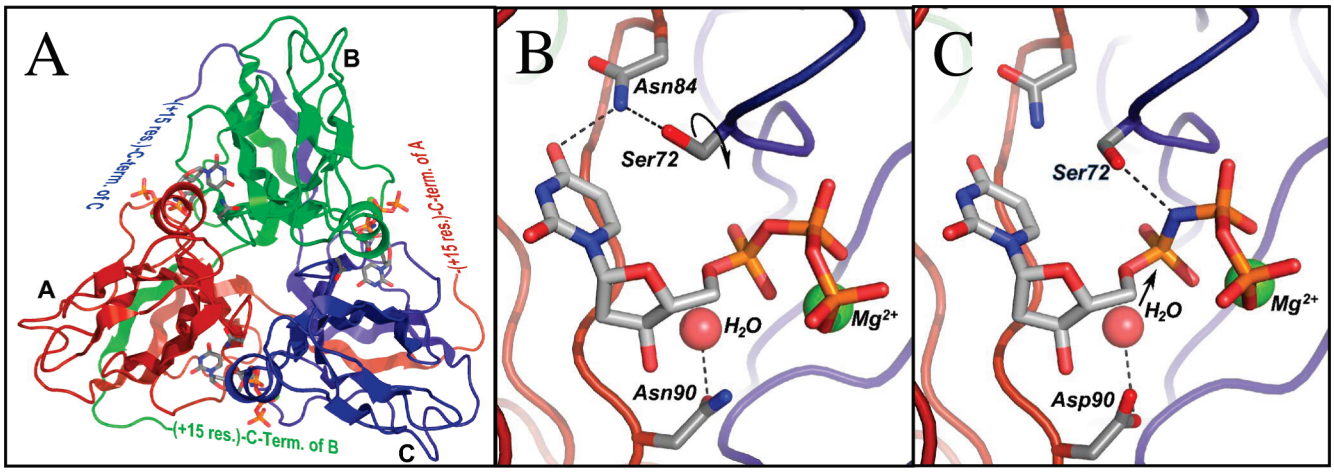

FIGURE 1: *E. coli* dUTPase, structure, catalysis, and side chain conformational ambiguity (*10*). (A) The complex of the Asp90 → Asn mutant with dUTP•Mg is displayed to demonstrate the C3-symmetric architecture of the trimeric dUTPase (PDB 1syl). Note in particular the position of the active sites at the subunit interfaces and how all subunits participate in the formation of each of these sites. (B) Close-up of the Asp90 → Asn mutant active site region with bound substrate. The hydroxyl of the conserved Ser72 forms a hydrogen bond to Asn84 at the bottom of the pyrimidine pocket, which in turn is linked to the pyrimidine ring of the substrate (dashed lines). (C) The active site of the wild-type enzyme occupied by the substrate analogue α,β-imido-dUTP•Mg (PDB 1rn8). Here the side chain of Ser72 has rotated to bring the hydroxyl group within hydrogen bond distance of the α,β-bridging nitrogen of the analogue. As indicated by the arrow, the catalytic reaction is assumed to be initiated by the nucleophilic attack of a water molecule, which is enclosed at the active site and activated by the conserved Asp90 base. The pictures were generated with PyMol (DeLano Scientific).

The side chain of S72 exhibits conformational freedom in the apoenzyme (*16*)but is fixed in complexes with the substrate (*10*) and the substrate analogues α,β-imido-dUTP•Mg (*6, 10, 15*) and α,β-methylene-dUDP (*17*). However, the orientation of the side chain differs drastically depending on which ligand is bound to the enzyme The structures of the complexes formed with α,β-imido-dUTP•Mg and the trimeric dUTPases from *E. coli* and *Mycobacterium tuberculosis*, as well as with the monomeric EBV dUTPase, are essentially superimposable with respect to the analogue and the enzyme functional groups with which it interacts. Invariably, the nitrogen that bridges the α- and β-phosphorus of the analogue is engaged in a hydrogen bond to the β-OH of the conserved serine residue. The observation of this bond in the *M. tuberculosis* dUTPase complex led to the proposal that the serine β-OH promotes catalysis by balancing negative charge that develops at the α,β-bridging oxygen in the course of the reaction (*6*). However, in the complex of the D90N *E. coli* dUTPase with the substrate proper, the β-OH of S72 points away from the α,β-bridging oxygen and may form a hydrogen bond to the amide group of N84 at the bottom of the pyrimidine pocket (Figure 1B) (*10, 17*).

The dCTP deaminases, which in Gram-negative bacteria provide for a route of dUTP formation additional to the ribonucleotide reductase pathway, have a core and active site architecture homologous to that of the dUTPases (*18–20*). Interestingly, the dCTP deaminase of the thermophile *Methanocaldococcus jannaschii* is a bifunctional enzyme catalyzing the hydrolysis of the intermediate dUTP•Mg product by the same mechanism as the trimeric dUTPases (*21, 22*). Recently, the list of organisms that expresses such bifunctional dCTP deaminases has expanded to include the *M. tuberculosis* pathogen (*23*). The dUTPase active site residues "D90" and "S72" are conserved also in the dCTP deaminases, as is the conformational freedom of the serine side chain. In the strict deaminases an arginine side chain blocks the pocket for a putative dUTPase substrate water molecule, which explains why these enzymes do not catalyze hydrolysis of the dUTP•Mg product (*18*).

In the present study we have replaced the β-hydroxyl group of S72 at the active site of the *E. coli* dUTPase by hydrogen, effective in the S72A mutant, and probed the effects of the mutation on the properties of the enzyme. The results were at first surprising to us, in particular a drastically reduced K_M. But after dissecting the kinetics of the wild-type and mutant enzyme systems down to the magnitude of the individual rate constants and after probing the binding of metal-free dUTP and the α,β-imido-dUTP•Mg complex to the two enzyme forms and testing the latter as a substrate, a pattern emerged, which we believe is best explained by a dual and dynamic role for the conserved serine, in both the dUTPases and the bifunctional deaminases.

EXPERIMENTAL PROCEDURES

The genes coding for the enzymes used in this study were supplied in plasmids through the courtesy of Dr. Per-Olof Nyman (retired from Lund University, Lund, Sweden). If not otherwise indicated, chromatographic equipment and media were obtained from GE Healthcare Bio-Sciences AB, Uppsala, Sweden. The concentration of enzymes is given as the respective active site concentration throughout this paper.

Construction of the S72A E. coli dUTPase. The *E. coli* strains TG1 (supE thi-1 Δ(lac-proAB) Δ(mcrB-hsdSM)5 (r_K^- m_K^-) [F′ traD36 proAB $lacI^qZ\Delta M15$]) and BL21(DE3)pLysS (Novagen, U.K.) were used as hosts in all experiments, and the plasmid pET3a (Novagen, Madison, WI) was used as the expression vector. Restriction endonuclease *Dpn*I and DNA polymerase *pfu* Ultra were both obtained from Stratagene (La Jolla, CA). Nucleotides were from Roche (Mannheim, Germany), and the plasmid purification kit was from Qiagen (Basel, Switzerland). Other chemicals were of analytical grade and obtained from Sigma.

All cloning procedures were performed as described by Sambrook et al. (*24*). The *dUTPase* gene was amplified with

plasmid pET3a as template. Complementary oligonucleotides carrying mismatches for the specific modification as primers were obtained from MWG Biotech AG (Ebersberg, Germany). Except for the mismatches, the sense primer was identical to the coding strand of the *dUTPase* gene. Sense primer: 5′-CGG CAA TGA TGC TGC CGC GC**G** CCG GAT TGG GAC ATA AGC-3′. Antisense primer: 5′-GCT TAT GTC CCA ATC CGG **C**GC GCG GCA GCA TCA TTG CCG-3′. After digestion with *Dpn*I, the newly constructed plasmid was used to transform competent *E. coli* TG1 cells. The cells were spread over Luria−Bertani (LB) agar plates containing 100 μg/mL ampicillin. Colonies were selected randomly and sequenced using BigDye terminators version 3.0 from Applied Biosystems (Warrington, U.K.) according to the supplier's instructions. The results were analyzed on an ABI 3100 DNA sequencer by the BM unit at Lund University.

Expression of the S72A E. coli dUTPase. The plasmid containing the S72A dUTPase gene was used to transform *E. coli* BL21(DE3)pLysS competent cells according to a standard protocol (heat shock at 42 °C). Streaking on LB plates containing ampicillin (100 μg/mL) provided positive colonies of transformants. Shaking flasks containing 250 mL of LB medium with ampicillin (200 μg/mL) were each inoculated with transformed bacteria from an isolated single colony on the LB plate, and the flasks were incubated on a shaker at 37 °C. The bacteria were grown to an OD_{600} of 0.5−0.7 and then induced with IPTG to a final concentration of 1 mM. The induced cultures were incubated on the shaker at 37 °C for another 5 h. Cells were harvested by centrifugation at 6650*g* for 20 min at 4 °C, and the pellets were stored at −20 °C.

Extraction and Purification of the S72A E. coli dUTPase. The pellet obtained from a 250 mL culture was dissolved in 24 mL of extraction buffer, pH 7.5, containing Hepes (20 mM), NaCl (50 mM), EDTA, EGTA, DTT, PMSF (all 1 mM), and glycerol (10%). The cells were lysed, and their content was extracted by three cycles of freezing and thawing, followed by three cycles of sonication on ice (60 mA for 2 min). The resulting suspension was centrifuged at 6650*g* for 45 min at 4 °C. The clear extract in the supernatant was stored at −20 °C.

The bacterial extract was subjected to chromatography on phosphocellulose (P11; Whatman International Ltd., England) (*25*) packed in a XK26 column. The column was preequilibrated with a pH 5.5 buffer, containing NaCl (0.04 M), sodium acetate (20 mM), and DTT (1 mM), and developed with a linear gradient in NaCl (0.04−1.0 M) in the same buffer. Chromatographic fractions were analyzed by SDS−PAGE (Mini PROTEAN 3; Bio-Rad). Fractions containing highly purified dUTPase were combined, and the protein content was fractionated with ammonium sulfate. The fraction that precipitated in the 35−75% range of ammonium sulfate saturation was collected by centrifugation and redissolved in a minimum volume of the buffer described above. The dissolved protein was stored at −20 °C.

The purified mutant dUTPase fraction was analyzed by SDS−PAGE (*26*). The mutant active site concentration was determined ultimately through a kinetic titration procedure described in the Results section. The other dUTPases used in this study, i.e., the *E. coli* wild-type and the equine infectious anemia virus (EIAV) dUTPases, were produced and analyzed by identical, or similar (*25*), protocols. The concentrations of the *E. coli* dUTPases and the EIAV dUTPase preparations were determined spectrophotometrically using the extinction coefficients 0.51 mL mg^{-1} cm^{-1} and 15300 M^{-1} cm^{-1}, respectively (*27, 28*).

Prior to each experiment the frozen dUTPase solution was thawed on ice and desalted on a PD-10 column equilibrated with the appropriate buffer. The desalted stock was subsequently diluted into the buffer system of the experiment. The assay, frontal chromatography, and viscosity measurements were carried out at a constant ambient temperature in the range 23−25 °C.

Activity Assay. The purified mutant dUTPase (0.5 μM) was incubated with dUTP (60 μM) in a pH 7.5 buffer, containing $MgCl_2$ (5 mM), Hepes (0.025 M), and NaOH (∼0.0125 M), and adjusted to 0.1 M ionic strength with KCl (=buffer A). The reaction mixture was transferred to a syringe attached to the loading loop of an FPLC system (Äkta Explorer). At timed intervals, 1.0 mL aliquots of the reaction mixture were subjected to analysis by ion-exchange chromatography on Q-Sepharose (HiTrap, 5 mL), using a linear 0.04−1.0 M NaCl gradient in buffer A, lacking $MgCl_2$, for elution. The same technique was applied to measure the rate of hydrolysis of the α,β-imido-dUTP·Mg complex (20 μM) in the absence and presence of the wild-type dUTPase (4 and 8 μM) and the S72A mutant (4 μM). The well-separated dUMP and dUTP elution peaks were integrated, and the area of the respective peak was divided by the total peak area and multiplied by 60 (=$[dUTP]_0$) to obtain the amount of product formed and substrate remaining. The former was plotted against time to obtain the progress of the reaction. The dUTP and dUMP positions in the chromatograms were determined by running a mixture of the respective pure nucleotide over the column.

Control of Endogenous Expression. To evaluate the expression of the endogenous dUTPase in the *E. coli* BL21(DE3)pLysS *cells*, the expression procedure was repeated twice using one pET3a plasmid lacking the *dut* gene and one carrying the S72A *dut* gene with an additional point mutation (manuscript in preparation). The proteins of the cells were extracted, purified, and analyzed using the same protocols as described above.

Frontal Chromatography. The S72A dUTPase was immobilized on agarose in prepacked columns (HiTrap, 1 mL NHS-activated) following the procedure recommended by the manufacturer. In brief, each column was incubated with solutions of S72A dUTPase (50 nmol active sites) in 1 mL 0.1 M Hepes/NaOH, pH 8.3. Columns thus prepared were attached, three in series, to the FPLC system. Solutions of dUTP (1−5 μM) or α,β-imido-dUTP (2−6 μM), in a pH 7.5 buffer containing Hepes 10 mM, NaOH (∼4 mM), and Na_2EDTA (1 mM), and with the ionic strength adjusted to 0.1 M with KCl, were run through the columns, and the elution volume for the ligand was determined at each concentration. Binding of the monoprotonated form of dUTP was studied at pH 6.0 (MES, 10 mM; KCl, 80 mM; Na_2EDTA, 1 mM). Binding of the α,β-imido-dUTP·Mg complex was probed by excluding EDTA and including $MgCl_2$ (5 mM) in the ligand solution. The effective void volume of the system was determined by running a solution of ATP through the column, at otherwise identical conditions.

Under the conditions described, ATP shows no binding to the *E. coli* wild-type dUTPase (*11*).

Protein Fluorescence. The fluorescence excitation spectrum of the S72A mutant was recorded at 25 °C on a Fluoromax 3 fluorescence spectrophotometer (Horiba Jobin Yvon), with the enzyme dissolved to 4 μM in buffer A. The emission wavelength was set to 335 nm, and the excitation and emission bandwidths were set to 1 and 5 nm, respectively. The effect of substrate binding on the spectrum was measured by making the enzyme solution 8 μM in dUTP. The spectrum was recorded within 100 s to ensure that sufficient dUTP remained to keep the mutant saturated.

Steady-State Kinetic Characterization of S72A. The activity of the S72A mutant was studied at 25 °C by monitoring the changes in the intrinsic protein fluorescence ($\lambda_{ex} = 275$ nm, $\lambda_{em} = 335$ nm). The corresponding signal has been used to study the transient state kinetics of substrate binding to the EIAV dUTPase (*29*). The reactions were initiated by mixing dUTP (6−10 μM) with the mutant (2−4 μM) in the presence of saturating $MgCl_2$ (5 mM). The inhibition of wild-type and S72A *E. coli* dUTPase by α,β-imido-dUTP·Mg was studied spectrophotometrically using the pH indicator method with cresol red as reporting agent (*11*).

Viscosity Effects. The pH indicator method was applied for measurements of the effects of viscosity on the reaction catalyzed by the *E. coli* and EIAV wild-type dUTPases. The bacterial and viral enzymes, at 0.12 and 0.015 μM, respectively, were reacted with dUTP, at 2 and 4 μM, respectively, in a pH 8 reaction medium containing $MgCl_2$ (5 mM), cresol red (25 μM), Bicine (50 μM), and KCl to adjust the ionic strength to 0.1 M. The viscosity of the medium was regulated by the inclusion of sucrose to final concentrations in the range 0−50% (w/w), in both the enzyme and substrate solutions. The viscosity at each sucrose concentration was obtained from published tables (*30, 31*). Relative viscosities were calculated as η/η_0, where η is the viscosity of the aqueous sucrose solution and η_0 the viscosity of pure water, both valid at the temperature of the experiment.

Substrate Binding Kinetics. The transient state kinetics of substrate binding to the S72A mutant dUTPase was studied at pH 7.5 by stopped-flow fluorometry using a SF-61DX2 instrument (Hi-Tech Ltd., Salisbury, U.K.). The enzyme (2 and 4 μM) was reacted with dUTP (6 and 12 μM) both dissolved in a reaction buffer (Hepes, 20 mM; NaOH, ~10 mM) containing $MgCl_2$ (5 mM) and KCl (85 mM). The reaction mixture was excited at 275 nm and the emission observed through a 330 nm cut-on filter. A Durrum D-100 stopped-flow instrument was used for a direct comparison of the kinetics of substrate binding to the wild-type and S/2A mutant dUTPases. For reasons explained below, the latter studies were performed at pH 6, by mixing the respective dUTPase, at 2 and 4 μM, with dUTP and $MgCl_2$, both at 20 μM. Bromocresol purple (50 μM) was used as reporting agent and Mes (50 μM) as the adjuvant buffer (*11*). The ionic strength was adjusted to 0.1 M by the inclusion of KCl. The reactions were monitored at 590 nm.

Thermal Stability of Wild-Type and S72A dUTPase. Each form of the enzyme was dissolved to a final concentration of 2 μM in 2.5 mL of a 10 mM Hepes buffer, pH 7.5, containing KCl (80 mM). The fluorescence of the respective dUTPase solution was monitored in the temperature range 25−80 °C under continuous heating and stirring. The temperature was measured with a thermistor submersed into the cuvette solutions. In a second study, the solutions were equilibrated at stepwise higher temperatures, and the fluorescence was registered at each step.

Stability toward Guanidine Hydrochloride. The kinetics of GuHCl-induced denaturation of the two *E. coli* dUTPase forms was studied at pH 7.5, 4 °C, using the intrinsic protein fluorescence as signal, by mixing enzyme into solutions of GuHCl at various concentrations (1.5−4 M). The final concentration of enzyme was 1 μM.

Data Analysis and Parameter Evaluation. Rate and equilibrium parameters were evaluated by nonlinear, or linear, regression using SigmaPlot or Dynafit (*32*). Specifically, the program Dynafit was applied for evaluating complete reaction progress curves obtained in the fluorescence studies on the S72A kinetics and in the stopped-flow studies on the effects of viscosity on the kinetics of the reactions catalyzed by the *E. coli* and EIAV wild-type dUTPases. Using a numerical approach, Dynafit is capable of fitting the differential equations describing the rate of change of the species in the mechanistic model applied, which in this study is the Michaelis−Menten mechanism.

RESULTS

Mutant Isolation and Purification. The purified S72A dUTPase fraction was analyzed by SDS−PAGE. Except for minor impurities, the gel revealed a single major band that ran in parallel with the wild-type *E. coli* dUTPase reference.

Activity Assay. The mutant active site concentration was calculated based on the 280 nm absorbance and a purity of 85%, as estimated by SDS−PAGE. The time course of the reaction, measured chromatographically, was linear until completion. It indicated a k'_{cat} for the mutant of 0.008 s^{-1}, a number reduced more than 700 times compared to that reported for the wild-type enzyme (*11*). A prime, as above in k'_{cat}, will be used to distinguish rate and equilibrium constants that characterize the mutant from those that characterize the wild-type enzymes. The chromatograms further revealed that dUTP and dUMP were the only nucleotides present during the hydrolysis process.

Binding of Metal-Free dUTP to S72A. When solutions of dUTP or ATP, containing EDTA to quench divalent metal ion activity, were run over the column with immobilized S72A, dUTP was retarded by the column whereas ATP was not, indicating specific binding of metal-free dUTP to the mutant enzyme (Figure 2, inset). The number of dUTP molecules bound to the immobilized mutant is given by $(V - V_0)C_{dUTP}$. Here C_{dUTP} is the concentration of dUTP in the liquid applied to the column, V_0 is the column void volume, as determined with ATP, and V the volume of the column eluate preceding the dUTP front. The latter depends on C_{dUTP} according to eq 1 (*33*).

$$V - V_0 = \frac{N_E}{K_{E\cdot dUPT} + C_{dUPT}} \quad (1)$$

In eq 1, N_E is number of immobilized mutant binding sites and $K_{E\cdot dUTP}$ is the equilibrium constant for dissociation of the S72A·dUTP complex. Using eq 1, the data in Figure 2 were evaluated by nonlinear regression. This gave $N_E = 11.7 \pm 0.5$ nmol and $K_{E\cdot dUTP} = 13.4 \pm 0.7$ μM. The latter number is close to that (16 μM) reported for the dissociation of the

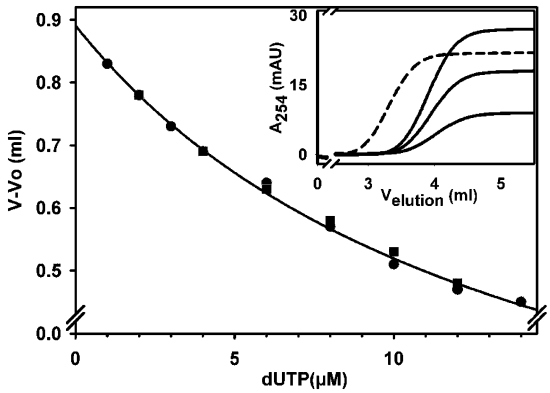

FIGURE 2: Frontal chromatography of metal-free dUTP on S72A dUTPase. The inset shows the ascending part of the elution profiles of ATP (2 μM, dashed line) and dUTP (from left to right: 6, 4, and 2 μM, solid lines). The main panel shows the dependence of the retention volume on the concentration of dUTP in the injected solution. The plot combines data from two separate measurements as indicated by different symbols.

Scheme 1

$$E + S \underset{k_{-1}}{\overset{k_1}{\rightleftharpoons}} ES \xrightarrow{k_{cat}} E + P$$

corresponding complex formed with the wild-type enzyme and which was determined by an indirect kinetic method (*11*).

Determination of k'_{cat}. Studies on the homotrimeric dUTPases have shown that their kinetic behavior is adequately described by the Michaelis−Menten mechanism (with the Briggs−Haldane extension) (Scheme 1) and that this can be applied to analyze complete reaction progress curves (*11, 29, 34*).

These studies have shown that K_M is more than 2000 times lower than the K_i (0.7 mM) of the combined dUMP and pyrophosphate products (*11*). For this reason, the time derivative of progress curves that provide information on both k_{cat} and K_M is given by the Michaelis−Menten rate equation throughout the complete reaction.

In search of a suitable signal, fluorescence excitation spectra of S72A were recorded in the absence and presence of dUTP and Mg^{2+} at saturating concentrations. The spectra demonstrated that binding of dUTP·Mg to S72A causes a 15% quench of the protein fluorescence ($\lambda_{ex} = 275$ nm; data not shown). This quenching was used as a signal to monitor the reaction catalyzed by the mutant preparation, through the appearance of free S72A. Curve A in Figure 3 was obtained by reacting S72A (4 μM) with dUTP (10 μM) in the presence of Mg^{2+} (5 mM). It displays an extensive zero-order lag, indicating 1.5 rounds of enzyme turnover at $C_S \gg K'_M$, abruptly followed by a first-order rise toward the maximum fluorescence, reflecting the release of free mutant in a last single turnover of the system at $C_E \gg K'_M$. Under such circumstances, the data cannot be used for an evaluation of K'_M, but the time constant of the exponential transient is a close estimate of k'_{cat} (*11*). This was evaluated to 0.008 s^{-1} by nonlinear regression, confirming the number obtained for k'_{cat} in the activity assay, and identical to the number obtained by numerical fitting of Scheme 1 to the complete trace, using Dynafit.

Determination of K'_M. Two experiments were designed specifically for this purpose. First we studied the effects on the progress of the reaction of including catalytic amounts

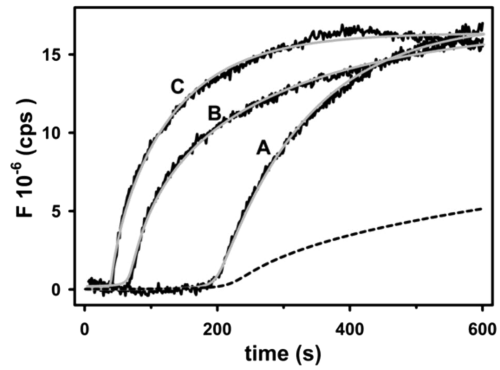

FIGURE 3: Hydrolysis of dUTP by the purified S72A mutant monitored by changes in the intrinsic protein fluorescence. The reaction was studied in the absence (curve A) and presence of added *E. coli* wild-type dUTPase at 0.025 (curve B) and 0.05 μM (curve C), respectively. The solid gray lines represent the kinetic model in Scheme 1 with the best fit rate constants. The dashed line is the course curve A would have taken if the activity observed derived from the *E. coli* endogenous dUTPase.

of the wild-type enzyme in the reaction mixture. As demonstrated by curves B and C in Figure 3, inclusion in the reaction mixture of increasing amounts of the wild-type dUTPase progressively shortened the lag phase and resulted in a significantly faster initial release of free mutant. The differential equations, defined by Scheme 1 for both the wild-type and mutant dUTPase reactions, were solved and fitted simultaneously to the experimental data in curves B and C using Dynafit. With the rate constants of the wild-type enzyme set to satisfy $k_{cat} = 5.8$ s^{-1} and $K_M = 0.21$ μM (*11*), this gave values for k'_{-1} in the range 0.05−0.6 s^{-1}, depending on the value of k'_1 used, but invariably $k'_{cat} = 0.008$ s^{-1}. Based on these values, and indifferent to the choice of k'_1, K'_M was calculated to be 0.006 μM. Simulation of the reactions using the best fit rate constants resulted in the solid gray lines drawn in Figure 3.

Second, the concentration of free Mg^{2+} in the reaction mixture was reduced and buffered with EDTA. This should result in an apparent increase in K'_M by a factor $(1 + K_{dUTP\cdot Mg}/[Mg^{2+}]_{buf})$, where $K_{dUTP\cdot Mg}$ is the equilibrium constant for dissociation of the dUTP·Mg complex and $[Mg^{2+}]_{buf}$ the EDTA-buffered concentration of free Mg^{2+}. This factor was determined by analyzing the effects of using EDTA in excess over Mg^{2+} on the reaction catalyzed by the wild-type dUTPase. With EDTA at 1 mM and $MgCl_2$ at 0.4, 0.6, and 0.75 mM, the apparent K_M increased 80, 43, and 24 times, respectively. The effects of using $MgCl_2$ reduced to 0.75 and 0.40 mM in the presence of 1 mM EDTA on the S72A reaction with dUTP are demonstrated in Figure 4. The apparent K'_M values governing the shape of curves B and C in Figure 4 were evaluated using Dynafit. The numbers obtained, 0.100 μM (B) and 0.534 μM (C), were divided by 24 (B) and 80 (C), respectively, to yield 0.0042 and 0.0067 μM, for K'_M.

Kinetic Titration of S72A Active Sites. With a K'_M that low, additions of S72A to solutions containing excess Mg^{2+}-saturated dUTP will result in an essentially stoichiometric occupation of the S72A sites by dUTP·Mg, such that $[dUTPMg] \approx C_{dUTP} - C_{E'}$. This was exploited to establish the mutant active site concentration based on the k'_{cat} evaluated above and the duration t_{zo} of the flat, zero-order, lag phase of the reaction as a function of the initial

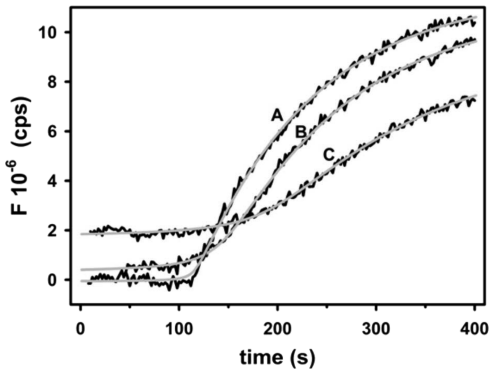

FIGURE 4: Hydrolysis of dUTP by the S72A mutant with the magnesium ion reduced and buffered at subsaturating levels. Curve A was obtained by reacting the mutant (4 μM) with dUTP (8 μM) at a saturating magnesium ion concentration (5 mM) and serves as a reference. Curves B and C were obtained with EDTA (1 mM) included in the reaction mixture and with the total magnesium ion concentration reduced to 0.75 and 0.4 mM, respectively. The gray lines represent the kinetic solution to the reaction in Scheme 1 using the best fit parameter values.

concentration of dUTP. The t_{zo} was determined using dUTP at six concentrations (data not shown) and $C_{E'}$ evaluated by fitting eq 2 to the experimental data (the corresponding double reciprocal plot was linear).

$$t_{zo} = \frac{C_{dUPT} - C_E}{k'_{cat} C_E} \quad (2)$$

This called for only a minor adjustment of the number determined spectrophotometrically for the assay.

Linking the Activity Observed to the Mutant. When working with mutant enzymes with drastically reduced activity, in particular if homologous expression is practiced, it is important to establish that the activity observed derives from the mutant and not from the endogenously produced enzyme, and several steps were taken to secure this link. The purified bacterial extract obtained from expression of the pET3a plasmid lacking the *dut* gene revealed the same sets of electrophoretic bands as the extracts containing the wild-type and S72A dUTPase forms, except for a distinct dUTPase band. When the fractions normally carrying the dUTPase were combined and incubated with the assay solution, hydrolysis of dUTP could not be detected even after 8 h of incubation. The purified double mutant dUTPase protein, obtained from expression of the S72A plasmid with an additional mutation in the *dut* gene, displayed no hydrolytic activity toward dUTP·Mg when incubated with the substrate for 8 h, at the same protein and substrate concentrations that were used to assay the S72A single mutant (manuscript in preparation). These results strongly suggest that the activity observed in the S72A extract derives exclusively from the mutant.

Moreover, because the data in Figure 3 were collected at $C_{E'} \gg K'_M$ (or the corresponding K'_d, had the mutant been inactive), it follows that the concentration of dUTP·Mg will become effectively buffered by equilibrium binding to the excess mutant as it is continuously hydrolyzed and reduced below $C_{E'}$. Under such circumstances, an endogenous dUTPase activity, capable of hydrolyzing only 6 μM free dUTP·Mg in 200 s, as indicated by the lag in curve A of Figure 3, cannot proceed to hydrolyze also those bound to S72A at the rate observed, and not at a rate that decreases

Table 1: (A) Kinetic Constants[a] Determined for the *E. coli* Wild-Type and S72A Mutant dUTPases and (B) Equilibrium Constants[a] Determined for the Dissociation of the Complexes Formed with the *E. coli* Wild-Type and S72A Mutant dUTPases and the Listed Ligands

	dUTP·Mg			
(A)	k_1 (μM^{-1} s^{-1})	k_{-1} (s^{-1})	k_{cat} (s^{-1})	K_M (μM)
wild type	42 ± 0.5[b] 47.6 ± 1.2[c]	6.2 ± 1.1[b]	5.8 ± 0.4[e]	0.21 ± 0.04[e]
S72A	17.0 ± 0.5[b] 17.3 ± 0.5[h]	0.10 ± 0.04	0.008 ± 0.002	0.006 ± 0.002

(B)	dUTP·Mg K_d (μM)	dUTP K_d (μM)	α,β-imido-dUTP·Mg K_d (μM)
wild type	0.15 ± 0.02[d] 0.13 ± 0.01[d]	16[f]	3.9 ± 0.5 5.0[g]
S72A	0.006 ± 0.002	13.4 ± 0.5	2.1 ± 0.5

[a] Except when otherwise indicated constants were determined at pH 7.5. All values represent the average of at least four independent measurements. [b] From substrate binding kinetics at pH 6. [c] From viscosity effects on K_M/k_{cat}. [d] Calculated as k_{-1}/k_1. [e] From ref *11* and confirmed here. [f] From ref *11*. [g] From ref *10*. [h] Determined by direct stopped-flow measurements.

exponentially with time. These facts are emphasized by the dashed line in Figure 3, which is the course the reaction would take if the activity were caused exclusively by a contaminating *E. coli* wild-type dUTPase. The curve was obtained using the simulation capability of Dynafit. It is based on the kinetic parameters of the *E. coli* wild-type dUTPase (*11*), the activity observed, and a K_d for dUTP·Mg binding to the S72A mutant equal to the K'_M reported in Table 1. Data obtained in a large number of measurements under different conditions with respect pH, metal ion, substrate, and enzyme concentration are constant with respect to the exponential nature of the fluorescence increase associated with the release of mutant active sites (for examples, see Supporting Information (SI)). Also, the fact that the rising portion in curves B and C in Figure 3 does not, as opposed to curve A, follow an exponential course shows that each of curves B and C is generated by the activity of two different enzymes, which compete for the common substrate.

Hence we conclude that the S72A mutation causes a 725-fold reduction in k_{cat} and a 35-fold reduction in K_M. Because $K_M = (k_{-1} + k_{cat})/k_1$, the entire reduction in K_M could result from the reduction in k_{cat}. This, however, requires that $(k_{-1} + 5.8)/(k_{-1} + 0.008) = 35$, by which k_{-1} evaluates to 0.16 s^{-1}. A k_{-1} that much lower than k_{cat} would make the wild-type dUTPase substrate interaction an unusually "sticky" one.

Kinetics of Substrate Binding to the S72A dUTPase. The quenching of the intrinsic protein fluorescence, caused by substrate binding to S72A, made it possible to follow the process in real time by stopped-flow fluorometry (Figure 5). The rate constants for the exponential fluorescence decay observed at excess concentrations of substrate, 6 and 12 μM, were 104.6 ± 3.2 and 231.2 ± 10.9 s^{-1}, respectively, hence indicating k'_1 to be 17 s^{-1} and 19 s^{-1}. Using these numbers, and those reported above for k'_{cat} (0.008 s^{-1}) and K'_M (0.006 μM), k'_{-1} evaluates to a number close to 0.1 s^{-1}.

Kinetics of Substrate Binding to the Wild-Type dUTPase. Attempts at using stopped-flow fluorescence for monitoring substrate binding to the wild-type enzyme failed because of a weaker signal and faster kinetics. In the pH range 6.5−8.5 substrate binding is pH neutral, precluding the pH indicator approach for transient state kinetic measurements. However,

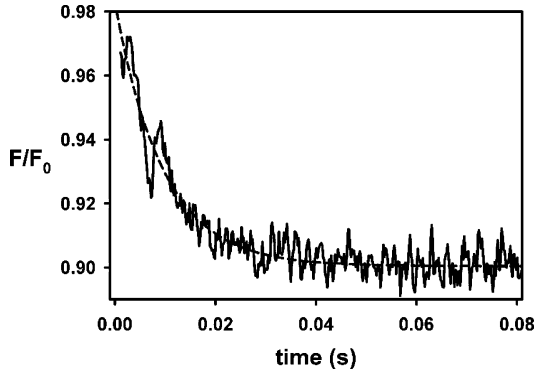

FIGURE 5: Stopped-flow fluorescence trace showing the time course of substrate binding to the S72A *E. coli* dUTPase at pH 7.5. The displayed graph represents the average of seven traces obtained by reacting the enzyme (2 μM) with dUTP·Mg^{2-} (6 μM). The dashed line represents an exponential decay function with the best fit rate constant 104 s^{-1}.

if k_{-1} is comparable to, or smaller than, k_{cat}, an estimate of k_1 can be obtained by determining K_M/k_{cat} as a function of the viscosity of the reaction medium (*35, 36*). This technique was applied to evaluate the kinetics of substrate binding to the wild-type dUTPase. Because of the indirect nature of the method, the study was expanded to include the effects of viscosity on the steady-state kinetics of the EIAV dUTPase. This enzyme is structurally and functionally homologous to the *E. coli* enzyme, and the rate constants defining its K_M (k_{-1}, k_1, and k_{cat}) have all been determined by direct methods (*29, 34*). The effects of medium viscosity on the kinetic properties of the *E. coli* and EIAV wild-type dUTPases were studied in parallel, using sucrose as the viscous agent. Complete reaction curves for the hydrolysis of dUTP·Mg (2 or 4 μM) by the respective dUTPase (0.1 or 0.05 μM) in a reaction medium of pH 8 (to permit comparison with the previously published data), containing from 0% to 50% (w/w) sucrose, were recorded by the pH indicator method (*11*) (see below). The reaction curves obtained with the *E. coli* enzyme are presented in Figure 6A. Data of the same quality were obtained using the EIAV enzyme. The k_{cat} and K_M values governing the shape of each curve were evaluated with Dynafit, using enzyme concentrations determined spectrophotometrically. The reciprocal catalytic efficiency, K_M/k_{cat}, was plotted against the relative viscosity (η_{rel}) of the medium and the slope and intercept of eq 3 (*36*) evaluated by linear regression (Figure 6B). (Alternative graphical representations of the data are available in SI.)

$$\frac{K_M}{k_{cat}} = \frac{k_{-1}}{k_{cat}k_1} + \frac{\eta_{rel}}{k_1} \quad (3)$$

With the EIAV dUTPase, the intercept and slope were 0.030 ± 0.001 and 0.0094 ± 0.002 μM s, respectively. That is, with the viral enzyme $k_1 = 106$ μM^{-1} s^{-1} and, using $k_{cat} = 25$ s^{-1} (*34*), $k_{-1} = 79$ s^{-1}, in close agreement with the data previously reported for this enzyme (*29*). With the *E. coli* dUTPase the intercept and slope were 0.023 ± 0.004 and 0.0210 ± 0.0005 μM s, which gave $k_1 = 47.6$ μM^{-1} s^{-1} and, using $k_{cat} = 5.8$ s^{-1}, $k_{-1} = 6.2$ s^{-1}.

A Comment on the Method. The pH indicator method used in this study to monitor the hydrolysis of dUTP is described in detail in ref *11*. In brief, a pH indicator is used to sense the release or uptake of protons associated with the reaction studied. An additional buffer can be included to limit the pH changes, protect against accidental changes in pH, and mask the buffer capacity of functional groups in the components of the system studied. The molecular indicator absorbance response is given by $\Delta A_i = q_i n \Delta\epsilon_i$, where n is the number of protons exchanged in the reaction, $\Delta\epsilon_i$ the difference between the molecular absorbance of the basic and acidic form of the indicator at the wavelength studied, and q_i, finally, the relative buffer capacity provided by the indicator. The method is conveniently applied to systems where the reaction can be followed to completion, such as the dUTPase system, because the molecular response coefficient can be calculated directly from ΔA_i and the substrate concentration used. It should be noted that each single trace in Figure 6A represents a large number of traditional initial rate measurements and covers concentrations of substrate ranging from well above K_M to zero. To emphasize this, the inverse of the first derivative of a reaction trace for the wild-type *E. coli* dUTPase was plotted as a function of the reverse residual substrate concentration, generating the Lineweaver−Burk diagram in Figure 7. The tendency to an upward curvature at high $[S]^{-1}$ is a consequence of the fact that the plot was generated using the total residual [S], which (with $C_E \approx K_M \approx 0.2$ μM) has a significant contribution from [ES] toward the end of the reaction. The latter fact makes a numerical fitting more appropriate than fitting of the implicit integrated rate equation.

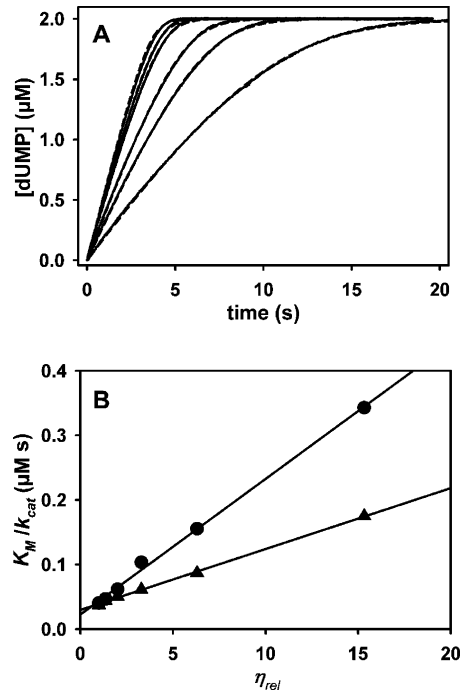

FIGURE 6: Effects of medium viscosity on the kinetics of the dUTPase reaction. The complete hydrolysis of dUTPMg by the *E. coli* and EIAV dUTPases was recorded at increasing medium viscosities, using sucrose (0−50%) as the viscous agent and a pH indicator (cresol red) as reporting agent. (A) The progress curves obtained with the *E. coli* enzyme as catalyst at (from left to right) 0%, 10%, 20%, 30%, 40%, and 50% sucrose. Data are shown as solid black lines and the best fit progress curves, based on the mechanism in Scheme 1, as dashed lines. (B) The linear dependence of the reciprocal catalytic efficiency (K_M/k_{cat}) of the *E. coli* (●) and EIAV (▲) dUTPases on the relative viscosity of the reaction medium (η_{rel}).

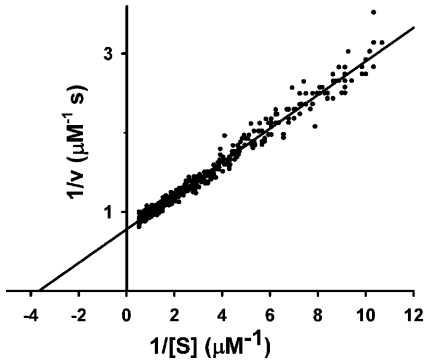

FIGURE 7: Lineweaver−Burk representation of a reaction trace, obtained with the pH indicator method by reacting the wild-type *E. coli* dUTase (0.2 μM) with dUTP·Mg (2 μM) in the standard reaction solution.

Direct Comparison of Substrate Binding Kinetics. The kinetics of dUTP·Mg binding to the wild-type and S72A *E. coli* dUTPases were studied in parallel under pseudo-first-order conditions. These studies were performed at pH 6 and with $MgCl_2$ reduced to 20 μM, both measures taken to provide a suitable signal. The pK_4 of the nucleotide phosphate moiety is 6.55 (*11*) so, at pH 6, the nucleotide will exist primarily as ($dUTPH^{3-}$). At the same pH, the K_d of the dUTP·Mg complex is increased ($1 + 10^{pK_4-pH}$) times, that is, from 47 to 214 μM, so, with dUTP also at 20 μM, there is essentially no preformation of dUTP·Mg. However, addition of enzyme to this system will trigger formation of the respective enzyme substrate complex and cause displacement of the substrate-bound H^+ in direct proportion to the amount of complex formed. The proton expelled is detected instantaneously by the pH indicator. To examine to what extent binding of $dUTPH^{3-}$ to the enzymes interferes with binding of the substrate proper, we determined K_d for binding of metal-free dUTP to the S72A dUTPase by frontal chromatography at pH 6.0. The number obtained (49 μM) indicates a much weaker binding of $dUTPH^{3-}$ than of $dUTP^{4-}$, and a maximum reducing effect on association rate constants of $1 + C_{dUTP}/K_d$, or 1.4. The kinetic properties of the wild-type dUTPase are not much altered over the pH range 6 − 9 (*11*), and there is little to suggest that the S72A mutant differ in this respect. We found that in the pH range 5.5−7.5, over which k_{cat} drops from 9 to 5.8 s^{-1}, k'_{cat} drops from 0.014 to 0.008 s^{-1} (this and related effects are documented in SI). As a precaution, the two reactions were studied in parallel and under identical conditions. As predicted, when the wild-type and S72A dUTPases each were mixed with the reaction solution described above, to final concentrations of 4 μM, this resulted in a pre-steady-state release of protons at exponentially decaying rates, as shown in Figure 8. The associated time constants, r, were evaluated by nonlinear regression using $A = A_0 + v_A t + \Delta A e^{-rt}$ as model for the reaction. In this model A is the absorbance at time t, ΔA the amplitude of the exponential phase of the reaction, $\Delta A + A_0$ the initial absorbance, and v_A the steady-state rate of absorbance change (set to 0 for evaluation of the reaction traces obtained with S72A). With the wild-type enzyme we obtained $r = 84$ s^{-1}, and with the S72A mutant we obtained $r = 29$ s^{-1}. The time constants were interpreted as shown by eq 4 (*11*).

$$r = k_1 \frac{C_{dUPT}}{1 + \dfrac{K_{dUPT\cdot Mg}}{[Mg^{2+}]}} + k_{-1} + k_{cat} \quad (4)$$

Because the factor $C_{dUTP}/(1 + K_{dUTP\cdot Mg}/[Mg^{2+}])$ was identical in the two experiments, the sum $k_{-1} + k_{cat} = 12$ s^{-1} was subtracted from the time constant obtained with the wild-type enzyme and k_1/k'_1 calculated to be 72/29 = 2.5. Using this ratio and $k_1 = 47.6$ μM^{-1} s^{-1}, as determined in the viscosity measurements, k'_1 calculates to 19 μM^{-1} s^{-1}. Direct evaluation of k_1 and k'_1 by multiplying 72 and 29, respectively, with $(1 + K_{dUTP\cdot Mg}/[Mg^{2+}])/C_{dUTP}$ gave $k_1 = 42$ μM^{-1} s^{-1} and $k'_1 = 17$ μM^{-1} s^{-1}. Taking into account the inhibition by $dUTPH^{3-}$, these numbers convert to 59 and 24 μM^{-1} s^{-1}, respectively. Application of the viscosity method on the wild-type enzyme at pH 6 gave $k_1 = 66$ μM^{-1} s^{-1}. The numbers thus derived for k'_1 are all consistent with the number (17 s^{-1}) obtained by the direct stopped-flow fluorometric measurement.

Thermal Denaturation Studies. The intrinsic fluorescence of the wild-type and S72A dUTPase forms decreased sigmoidally with temperature (Figure 9). Taking the point of inflection of each curve as the respective transition temperature, we have 48 °C for the wild-type enzyme and 60 °C for the mutant. The former temperature is close to the 49 °C reported earlier to represent a nonenthalpic transition in the wild-type dUTPase (*37*). The reversible or nondestructive nature of the process was confirmed by incubating the respective enzyme at 60 °C for 10 min followed by activity measurements at 25 °C. The activity of both enzyme forms was retained completely following this treatment (SI). Repeating the incubation at 70 °C led to precipitation of both enzyme forms, consistent with a melting

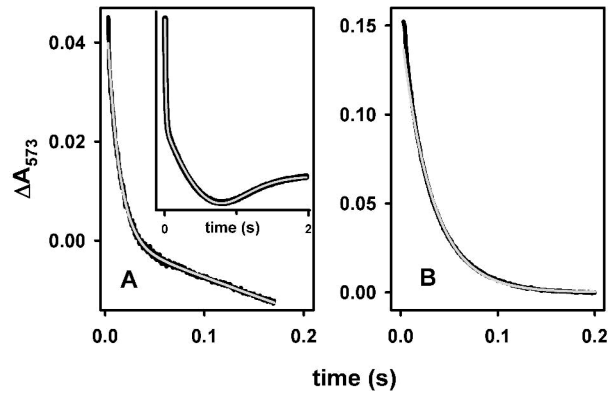

FIGURE 8: Comparative kinetics of formation of the enzyme−substrate complexes of the wild-type and S72A *E. coli* dUTPases. The black curves in panels A and B show the pH indicator absorbance changes triggered at pH 6 by reacting dUTP (20 μM) with the wild-type and S72A mutant dUTPase, respectively, both at 4 μM and in the presence of Mg^{2+} (20 μM). The gray lines represent the kinetic models with the best fit parameter values. The inset in panel A displays the pH indicator absorbance changes associated with the complete reaction catalyzed by the wild-type enzyme. Under the conditions prevailing the net reaction is best described by $dUTPH^{3-} + H_2O \rightarrow dUMPH^- + (1 - n)H_2PP_i^{2-} + nHPP_i^{3-} + nH^+$, where $n < {}^1/_2$. This explains the pH drop in the multiple turnover "steady-state" phase of the reaction. The initial drop reflects the displacement of the substrate-bound H^+ upon formation of the dUTPase−dUTP·Mg complex. Toward the end of the reaction the main event is the decomposition of this complex, which results in the uptake of $1 - n$ protons, consistent with the ascending tail of the course in the inset.

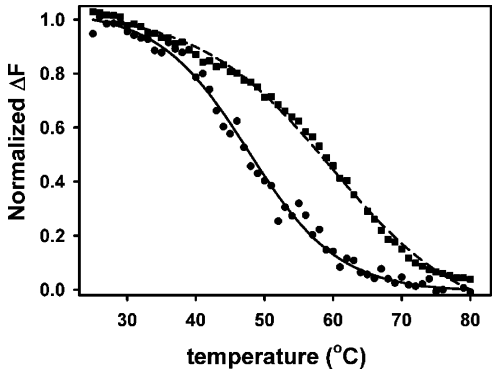

FIGURE 9: The effect of temperature on the intrinsic fluorescence of the wild-type (●) and S72A (■) *E. coli* dUTPases.

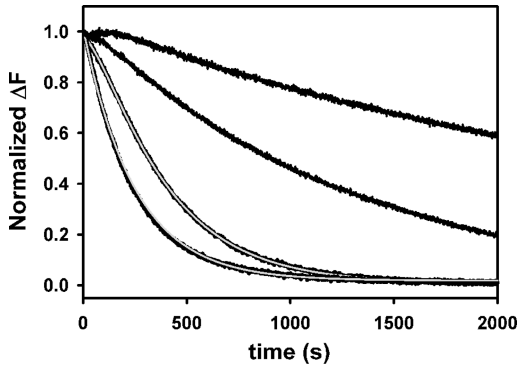

FIGURE 10: Fluorescence traces demonstrating different kinetics of the denaturation of the wild-type and S72A *E. coli* dUTPases at 4 °C by GuHCl. The upper two traces were recorded at 1.5 M and the lower two at 2.0 M GuHCl. In both sets, the upper trace represents the S72A mutant form of the dUTPase. A double and single exponential decay function was fitted to respectively the S72A and wild-type traces recorded at 2.0 M GuHCl, and the best fitted functions are superimposed as gray lines on the data traces.

temperature of 74 °C, reported for the wild-type *E. coli* dUTPase (*37*).

Stability toward Guanidine Hydrochloride. At all concentrations of the chaotropic agent tested (1.5, 2.0, 2.5, and 4.0 M) most of the fluorescence decrease followed a single exponential decay function with a rate constant that was about twice as high for the wild type as for the mutant form, indicating that the mutant is the more stable of the two forms. Apart from the rate difference, at 2 M GuHCl, the fluorescence change of the mutant was initiated by a lag phase (Figure 10) that could be observed with the wild type only at the lowest concentration of GuHCl tested and where it was even more extensive with the mutant form.

Binding of α,β-Imido-dUTP·Mg. The K_i for inhibition of the wild-type *E. coli* dUTPase by the analogue was determined to 3.9 μM, in agreement with the number (5 μM) previously reported (*10*). At 50 μM, the analogue had no obvious effect on the hydrolysis of dUTP·Mg (10 μM) by the S72A mutant (4 μM), indicating that binding of the analogue to the *E. coli* dUTPase is not significantly enhanced by the mutation. Consistently, the K_d for binding α,β-imido-dUTP·Mg to the mutant was determined by frontal chromatography to be 2.1 μM. The fact that the activity linked to the mutant is not significantly affected by the inhibitor, at a concentration that causes an apparent 14-fold increase in K_M for the wild-type dUTPase (to 3 μM), clearly indicates that an endogenous dUTPase does not contribute to this activity.

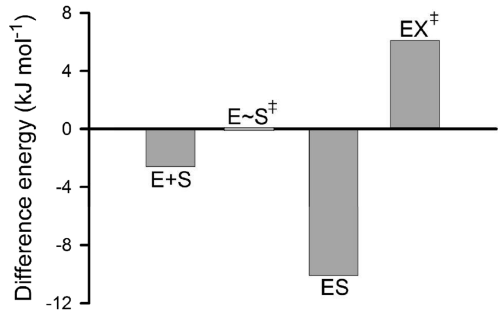

FIGURE 11: Difference energy diagram, showing the effects of changing serine 72 in the *E. coli* dUTPase to an alanine on the energy of the reactant states in the dUTPase reaction. The states are the free reactants (E + S), the transition state in substrate binding (E~S‡), the enzyme substrate ground state (ES), and transition state (EX‡) complexes. If the 2.8-fold reduction in k_1 results from a destabilization of E~S‡, rather than a stabilization of E + S, as indicated here, the corresponding 2.6 kJ of energy should be added to each bar.

Hydrolysis of α,β-Imido-dUTP. The analogue (20 μM) was spontaneously hydrolyzed, and dUMP was the only nucleotide product detected by chromatography. Assuming a first-order and complete decay, the rate constant was calculated to $\sim 1 \times 10^{-6}$ s^{-1} based on the linear first 5% of the reaction. The rate was not affected by the addition of the S72A dUTPase (4 μM) but was reduced to about 0.7 and 0.6 $\times$ 10^{-6} s^{-1} in the presence of 4 and 8 μM wild-type dUTPase. The inability of the *E. coli* dUTPase to catalyze the hydrolysis of the analogue contrasts to an earlier report, which states that this occurs with a k_{cat} of 2×10^{-5} s^{-1}, but which does not consider the spontaneous hydrolysis (*10*).

Summary of Results. Rate and equilibrium binding data for the *E. coli* wild-type and S72A mutant dUTPases are presented in Table 1. The effect of the S72A mutation on the energies of the reactant states in the dUTPase reaction were calculated based on the data in Table 1 and are shown by the difference energy diagram in Figure 11.

DISCUSSION

A serine is strictly conserved at the active site of the monomeric and trimeric dUTPases, as well as at the active site of the likewise trimeric dCTP deaminases. To disclose the role in substrate binding and catalysis of the conserved serine side chain, we replaced S72 in the well-studied *E. coli* dUTPase with an alanine. Our results show that, with the hydroxyl group of the wild-type enzyme in place of the hydrogen of the alanine mutant, k_{cat} is drastically enhanced. They also show that this enhancement is caused as much by a destabilization of the reactant ground state as by a stabilization of its transition state (Scheme 2).

The opposing effects of the serine hydroxyl on the stability of the two reactant states are not covered by the *uniform*, *specific*, or *differential* binding effect of a functional group discussed in the literature (*38–40*). The possibility that the energetically opposite but catalytically cooperative effects of the S72 hydroxyl group are exercised at different positions will be discussed with reference to structural information available and experimental support obtained here.

Scheme 2

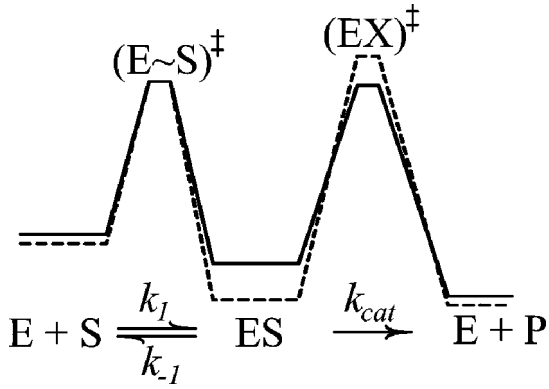

Based on our observation that S72A (E′) is more stable than the wild-type enzyme (E), both against a thermal transition in the molecule and GuHCl-induced denaturation, we conclude that some folding or assembly energy is used to bring S72 into its position. From the atomic resolution structure of the unligated *E. coli* dUTPase (*16*) we learn that the serine side chain reaches freely into a water-filled cleft between the subunits, where it exhibits considerable conformational freedom. It is thus not obvious how the β-OH interferes with the folding or assembly of the protein. We suggest, however, that with a hydrogen in place of the polar hydroxyl, fewer water molecules are retained at the subunit interface permitting a closer packing of the subunits, which stabilizes the protein and causes it to associate more slowly with its substrate (it is not a farfetched thought that the transition states in enzyme denaturation and substrate binding have features in common). However that may be, the destabilizing effect of the β-OH on the free enzyme is consistent, both with the observation that mutations that stabilize enzymes also reduce their catalytic efficiency (*41*) and with the view that polar groups are assembled into the active site at the expense of folding energy (*42*).

The S72A mutation caused a net increase in substrate binding energy of $RT \ln(k_{-1}k'_1/(k_1k'_{-1}) \approx 8$ kJ mol^{-1}. This effect was shown to depend on the presence of the Mg^{2+} ion, which also appears to be required to bind the flexible C-terminus on top of the active site in the bacterial dUTPase enzyme substrate complexes (*6*). We take this to indicate that the stronger binding in E′S compared to ES depends on interactions involving primarily the flexible C-terminus. The question then arises how this can be accomplished by removing the β-OH of S72. Our interpretation is that a more favorable interaction with the C-terminus in E′S is made possible by a narrowing of the intersubunit cleft. Now, assuming that the hydroxyl group occupies the same position in ES as in the D90N *E. coli* dUTPase−dUTP·Mg complex (Figure 1B), a narrowing of the cleft in ES would be prevented because of steric interference between the β-OH and the pyrimidine ring. At any rate, the ground state in ES is destabilized compared to E′S by at least[2] 8 kJ mol^{-1} and must stop at just encounter strain or stress, possibly toward the more narrow cleft and the more favorable interaction with the C-terminus that we presume is realized in E′S.

[2] If the higher k_1 of the wild-type enzyme results from a destabilization of the reactants, as indicated in Figure 11 and Scheme 2, rather than a stabilization of the transition state in substrate binding, then ES would be destabilized by $RT \ln(k_{-1}/k'_{-1}) \approx 10$ kJ mol^{-1} compared to E′S.

Regarding the orientation of the S72 side chain in ES, we argue that this is reproduced in the D90N dUTPase−dUTP·Mg complex. The alternative orientation, seen in complexes with the α,β-imido-dUTP·Mg substrate analogue, and which results in formation of a hydrogen bond between the serine β-OH and the α,β-bridging nitrogen of the analogue (Figure 1C), could depend on the imido group being the hydrogen donor, a possibility not previously discussed. This would be consistent with our observation that, whereas the analogue is spontaneously hydrolyzed at an appreciable rate, this reaction is not catalyzed by the *E. coli* dUTPase. The small effect of the S72A mutation on the binding of the analogue is likely to be apparent only; i.e., the loss of the hydrogen bond is compensated for by the same mechanism that accounts for the much stronger binding of the substrate in E′S than in ES.

The strain and stress encountered in ES would be of no value to catalysis unless relieved in EX‡, the enzyme transition state complex. We therefore suggest that a narrowing of the cleft occurs also in EX‡. The question then is how this is accomplished with the β-OH of the conserved serine in place? As a solution, we suggest that transition state formation in the dUTPase reaction involves a rotation of the S72 side chain around its $\alpha-\beta$ carbon bond that brings the hydroxyl group out of the cleft and into a position equal or similar to that observed in the complexes of dUTPases with α,β-imido-dUTP·Mg (Figure 1C). In this new position, it may induce its second effect and electrostatically stabilize the transition state. This may involve formation of a hydrogen bond with the β-OH as donor, either to the α,β-bridging oxygen of the transition state or to a nonbridging oxygen of a pentacoordinated α-phosphorus.

The conformational ambiguity of the conserved serine side chain is observed also in the bifunctional dCTP deaminases: the β-OH of the *M. jannaschii* enzyme is hydrogen bonded to the α,β-bridging nitrogen of a bound α,β-imido-dUTP·Mg but points in an opposite direction in the corresponding complexes with dCTP and dUTP (PDB 2hxd). In the complex of an inactive mutant of the strict *E. coli* deaminase with dCTP·Mg (*18*), the position of the conserved serine β-OH equals that observed in the D90N dUTPase−dUTP·Mg complex, discussed above (*10*). In this position, it has been implicated to promote the deamination of the pyrimidine (*18*). As absolutely conserved, the serine side chain is likely to occupy the same position and have the same function in the productive dCTP·Mg complexes of all these dCTP deaminases. We suggest that the position of the conserved serine side chain determines the order of events in the bifunctional dCTP deaminases: only after the exchange of H_2O for NH_3 at the pyrimidine, the serine side chain is set free to promote the hydrolysis of the triphosphate moiety by the mechanism described above for the dUTPases.

In conclusion, we argue that the S72A mutation in the *E. coli* dUTPase has generated a "transition state analogue" of the enzyme, which reacts with the substrate to release part of the energy normally released only upon formation of the enzyme transition state complex and which for this reason is catalytically compromised. We suggest that this effect is associated with interactions involving the flexible C-terminus. In view of the much tighter binding in E′S than in ES we postulate that the C-terminus is more intimately integrated with the active

site in E′S and exhibits a more transition state-like conformation than hitherto observed. Catalysis by the mutant is further compromised by the loss of a potentially transition state stabilizing polar group at the active site.

SUPPORTING INFORMATION AVAILABLE

Graphs describing (a) the dependence of pH on the activity of the *E. coli* S72A mutant dUTPase in the pH range 5−10.6, (b) the effect of enzyme concentration on the activity of the S72A mutant, (c) the effect on the wild-type and S72A dUTPase activities at 25 °C of exposing them to elevated temperatures in the range 20−60 °C, (d) the effects of viscosity on the activity of the S72A mutant, (e) a plot of $1/k_{cat}$ versus $1/\eta_{rel}$ (wild-type enzyme data), and (f) a plot of K_M/k_{cat} versus the concentration of sucrose (wild-type enzyme). This material is available free of charge via the Internet at http://pubs.acs.org.

REFERENCES

1. McIntosh, E. M., and Haynes, R. H. (1997) dUTP pyrophosphatase as a potential target for chemotherapeutic drug development. *Acta Biochim. Pol. 44*, 159–171.
2. Ladner, R. D. (2001) The role of dUTPase and uracil-DNA repair in cancer chemotherapy. *Curr. Protein Pept. Sci. 2*, 361–370.
3. Grässer, F. A., Romeike, B. F., Niedobitek, G., Nicholls, J., and Kremmer, E. (2001) dUTPase in human neoplastic cells as a potential target for therapeutic intervention. *Curr. Protein Pept. Sci. 2*, 349–360.
4. Mol, C. D., Harris, J. M., McIntosh, E. M., and Tainer, J. A. (1996) Human dUTP pyrophosphatase: uracil recognition by a beta hairpin and active sites formed by three separate subunits. *Structure 4*, 1077–1092.
5. Cedergren-Zeppezauer, E. S., Larsson, G., Nyman, P. O., Dauter, Z., and Wilson, K. S. (1992) Crystal structure of a dUTPase. *Nature 355*, 740–743.
6. Chan, S., Segelke, B., Lekin, T., Krupka, H., Cho, U. S., Kim, M. Y., So, M., Kim, C. Y., Naranjo, C. M., Rogers, Y. C., Park, M. S., Waldo, G. S., Pashkov, I., Cascio, D., Perry, J. L., and Sawaya, M. R. (2004) Crystal structure of the *Mycobacterium tuberculosis* dUTPase: Insights into the catalytic mechanism. *J. Mol. Biol. 341*, 503–517.
7. Prasad, G. S., Stura, E. A., McRee, D. E., Laco, G. S., Hasselkus-Light, C., Elder, J. H., and Stout, C. D. (1996) Crystal structure of dUTP pyrophosphatase from feline immunodeficiency virus. *Protein Sci. 12*, 2429–2437.
8. Dauter, Z., Persson, R., Rosengren, A. M., Nyman, P. O., Wilson, K. S., and Cedergren-Zeppezauer, E. S. (1999) Crystal structure of dUTPase from equine infectious anaemia virus; active site metal binding in a substrate analogue complex. *J. Mol. Biol. 285*, 655–673.
9. Barabás, O., Németh, V., and Vértessy, B. G. (2006) Crystallization and preliminary X-ray studies of dUTPase from Mason-Pfizer monkey retrovirus. *Acta Crystallogr., Sect. F: Struct. Biol. Cryst. Commun. 62*, 399–401.
10. Barabás, O., Pongrácz, V., Kovári, J., Wilmanns, M., and Vértessy, B. G. (2004) Structural insights into the catalytic mechanism of phosphate ester hydrolysis by dUTPase. *J. Biol. Chem. 41*, 42907–42915.
11. Larsson, G., Nyman, P. O., and Kvassman, J. O. (1996) Kinetic Characterization of dUTPase from *E. coli*. *J. Biol. Chem. 271*, 24010–24016.
12. Camacho, A., Arrebola, R., Peña-Diaz, J., Ruiz-Pérez, L. M., and González-Pacanowska, D. (1997) Description of a novel eukaryotic deoxyuridine 5′-triphosphate nucleotidohydrolase in *Leishmania major*. *Biochem. J. 325*, 441–447.
13. Hidalgo-Zarco, F., and González-Pazanowska, D. (2001) Trypanosomal dUTPases as potential targets for drug design. *Curr. Protein Pept. Sci. 2*, 389–397.
14. Moroz, O. V., Harkiolaki, M., Galperin, M. Y., Vagin, A. A., González-Pacanowska, D., and Wilson, K. S. (2004) The crystal structure of a complex of *Campylobacter jejuni* dUTPase with substrate analogue sheds light on the mechanism and suggests the "basic module" for dimeric d(C/U)Tpases. *J. Mol. Biol. 342*, 1583–1597.
15. Tarbouriech, N., Buisson, M., Seigneurin, J. M., Cusack, S., and Burmeister, W. P. (2005) The monomeric dUTPase from Epstein-Barr virus mimics trimeric dUTPases. *Structure 13*, 1299–1310.
16. González, A., Larsson, G., Persson, R., and Cedergren-Zeppezauer, E. (2001) Atomic resolution structure of *Escherichia coli* dUTPase determined ab initio. *Acta Crystallog., Sect. D: Biol. Crystallogr. 57*, 767–774.
17. Kovári, J., Barabás, O., Varga, B., Békési, A., Tölgyesi, F., Fidy, J., Nagy, J., and Vértessy, B. G. (2007) Methylene substitution at the alpha-beta bridging position within the phosphate chain of dUDP profoundly perturbs ligand accommodation into the dUTPase active site. *Proteins 71*, 308–319.
18. Johansson, E., Fanø, M., Bynck, J. H., Neuhard, J., Larsen, S., Sigurskjold, B. W., Christensen, U., and Willemoës, M. (2005) Structures of dCTP deaminase from *Escherichia coli* with bound substrate and product: reaction mechanism and determinants of mono- and bifunctionality for a family of enzymes. *J. Biol. Chem. 280*, 3051–3059.
19. Johansson, E., Bjornberg, O., Nyman, P. O., and Larsen, S. (2003) Structure of the bifunctional dCTP deaminase-dUTPase from *Methanocaldococcus jannaschii* and its relation to other homotrimeric dUTPases. *J. Biol. Chem. 278*, 27916–27922.
20. Huffman, J. L., Li, H., White, R. H., and Tainer, J. A. (2003) Structural basis for recognition and catalysis by the bifunctional dCTP deaminase and dUTPase from *Methanococcus jannaschii*. *J. Mol. Biol. 331*, 885–896.
21. Björnberg, O., Neuhard, J., and Nyman, P. O. (2003) A bifunctional dCTP deaminase-dUTP nucleotidohydrolase from the hyperthermophilic archaeon *Methanocaldococcus jannaschii*. *J. Biol. Chem. 278*, 20667–20672.
22. Li, H., Xu, H., Graham, D. E., and White, R. H. (2003) The *Methanococcus jannaschii* dCTP deaminase is a bifunctional deaminase and diphosphatase. *J. Biol. Chem. 278*, 11100–11106.
23. Helt, S. S., Thymark, M., Harris, P., Aagaard, C., Dietrich, J., Larsen, S., and Willemoes, M. (2008) Mechanism of dTTP inhibition of the bifunctional dCTP deaminase:dUTPase encoded by *Mycobacterium tuberculosis*. *J. Mol. Biol. 376*, 554–569.
24. Sambrook, J., Fritsch, E. F., and Maniatis, T. (1989) *Molecular cloning: a laboratory manual*, 2nd ed., Cold Spring Harbor Laboratory Press, Cold Spring Harbor, NY.
25. Persson, R., Nord, J., Roth, R., and Nyman, P. O. (2002) dUTPase from *Escherichia coli*; high-level expression and one-step purification. *Prep. Biochem. Biotechnol. 32*, 157–172.
26. Laemmli, U. K. (1970) Cleavage of structural proteins during the assembly of the head of bacteriophage T4. *Nature 227*, 680–685.
27. Hoffmann, I., Widstrom, J., Zeppezauer, M., and Nyman, P. O. (1987) Overproduction and large-scale preparation of deoxyuridine triphosphate nucleotidohydrolase from *Escherichia coli*. *Eur. J. Biochem. 164*, 45–51.
28. Bergman, A. C., Bjornberg, O., Nord, J., Rosengren, A. M., and Nyman, P. O. (1995) dUTPase from the retrovirus equine infectious anemia virus: high-level expression in *Escherichia coli* and purification. *Protein Expression Purif. 6*, 379–387.
29. Nord, J., Kiefer, M., Adolph, H. W., Zeppezauer, M. M., and Nyman, P. O. (2000) Transient kinetics of ligand binding and role of the C-terminus in the dUTPase from equine infectious anemia virus. *FEBS Lett. 472*, 312–316.
30. Mathlouthi, M. and Reiser, P. (1995) *SUCROSE Properties and Applications*, Blackie Academic and Professional/Chapman & Hall, 2-6 Boundary Row, London SE1 8HN, U.K.
31. Bubnik, Z., Kadlek, P., Urban, D., and Bruhns, M. (1995) *Sugar Technologists Manual: Chemical and Physical Data for Sugar Manufactures and Users*, Bartens Press.
32. Kuzmic, P. (1996) Program DYNAFIT for the analysis of enzyme kinetic data: application to HIV proteinase. *Anal. Biochem. 237*, 260–273.
33. Zhu, L., Chen, L., Luo, H., and Xu, X. (2003) Frontal Affinity Chromatography Combined on-Line with Mass Spectrometry: A Tool for the Binding Study of Different Epidermal Growth Factor Receptor. *Anal. Chem. 75*, 6388–6393.
34. Nord, J., Larsson, G., Kvassman, J. O., and Nyman, P. O. (1997) dUTPase from the retrovirus equine infectious anemia virus: Specificity, turnover and inhibition. *FEBS Lett. 414*, 271–274.
35. Kurz, L. C., Weitkamp, E., and Frieden, C. (1987) Adenosine deaminase: viscosity studies and the mechanism of binding of

substrate and of ground- and transition-state analogue inhibitors. *Biochemistry 26*, 3027–3032.
36. Schurr, M. J. (1970) The role of diffusion in enzyme kinetics. *Biophys. J. 10*, 717–727.
37. Takács, E., Grolmusz, V. K., and Vértessy, B. G. (2004) A tradeoff between protein stability and conformational mobility in homotrimeric dUTPases. *FEBS Lett. 566*, 48–54.
38. Albery, W. J., and Knowles, J. R. (1976) Free-energy profile of the reaction catalyzed by triosephosphate isomerase. *Biochemistry 15*, 5631–5640.
39. Fersht, A. (2003) *Structure and Mechanism in Protein Science*, 5th ed., W. H. Freeman and Co. Press, New York.
40. Kraut, D. A., Carroll, K. S., and Herschlag, D. (2003) Challenges in enzyme mechanism and energetics. *Annu. Rev. Biochem. 72*, 517–571.
41. Shoichet, B. K., Baase, W. A., Kuroki, R., and Matthews, B. W. (1995) A relationship between protein stability and protein function. *Proc. Natl. Acad. Sci. U.S.A. 92*, 452–456.
42. Warshel, A. (1998) Electrostatic origin of the catalytic power of enzymes and the role of preorganized active sites. *J. Biol. Chem. 273*, 27035–27035.

BI800325J